




Separating nucleation from growth for high-yield synthesis of thin silver nanowires

Yu Jiang¹, Ran Tao², Haotian Zhang¹, Neng Wan⁴, Ying Yang¹, Dawei Gu², Tianyou Zhang², Yunjun Rui^{1,2,3,*} , and Jun Xu^{3,*}

¹2011 College, Nanjing Tech University, Nanjing 210009, China

²Department of Physics, Nanjing Tech University, Nanjing 210009, China

³National Laboratory of Solid State Microstructures, Nanjing University, Nanjing 210093, China

⁴School of Electronic Science and Engineering, Southeast University, Nanjing 210096, China

Received: 19 July 2022

Accepted: 7 November 2022

Published online:

7 January 2023

© The Author(s), under exclusive licence to Springer Science+Business Media, LLC, part of Springer Nature 2023

ABSTRACT

Inactive gas (N₂ or Ar) and oxygen scavenger (Fe²⁺ or Cu⁺) are used for the synthesis of silver nanowires (AgNWs) with thin diameter (< 30 nm) and high aspect ratio (> 1000), but the yield is always low. Due to the oxidative etching, oxygen largely influences silver nanostructures not only in the nucleation process but also in the growth period. Herein, we systematically studied AgNW synthesis under the condition of an atmosphere with different oxygen contents (O₂, air, and N₂). We separated the formation of Ag-twinning seeds and nanoparticles in the incubation and the elongation of AgNWs in the growth, which are both sensitive to the oxygen content. AgNWs with 28.5 nm diameter, 2500 aspect ratio, and 91% yield were obtained when the sample was protected in N₂ (incubation) and refluxed with air (growth), resulting in a conductive film with a sheet resistance of 48 Ω/sq at a transmittance of 97.0%, comparable to that of ITO. The growth mechanism of such high-quality AgNWs was discussed.

1 Introduction

Silver nanowires (AgNWs) attract tremendous attention nowadays as the most promising materials for flexible transparent conductive film (TCF) electrodes widely used in liquid displays, touch screen, solar cells, and sensors [1–4]. To increase the transmittance in the visible region and decrease the sheet resistance of TCF, thin and long AgNWs are required.

High yield and repeatability of the synthesis are also desired for the large-scale production [5, 6].

It is well documented that the co-additives Cl⁻ and Br⁻ ions are typically applied to the polyol synthesis of AgNWs with very thin diameter and high aspect ratio [7–9]. The AgCl and AgBr crystal formed initially can not only serve as heterogeneous nucleants for the decahedral multiple-twinned particles (MTPs) with small size but also reduce the concentration of Ag⁺ ions in the solution, which is also beneficial to thin AgNWs. The diameters of 26 and 29 nm were

Address correspondence to E-mail: yjrui@njtech.edu.cn; junxu@nju.edu.cn

obtained by Zhang et al. and Wang et al., respectively [8, 9]. They both found that further increment of Br^- ions leads to AgNWs with decreased diameter but lower yield. For long AgNWs, it is necessary to decrease the oxygen content during the reaction process, because oxygen can absorb and dissociate on Ag surfaces, especially blocking (111) reactive sites from adding Ag atoms effectively. So the simplest way is using nitrogen (N_2) or argon gas (Ar) [5, 7, 10, 11]. By bubbling nitrogen gas during heating process, 20-nm AgNWs were prepared with aspect ratio up to 2000 [7]. On the other hand, Fe^{2+} and Cu^+ can act as O_2 scavengers, beneficial to the AgNW growth. The higher aspect ratio of 3000 was obtained under the coexistence of Cl^- , Br^- , and Fe^{2+} [9]. Korte et al. pointed that when the reaction is performed under an argon atmosphere and in the presence of Cu^+ , the resulting nanowires will be of smaller diameter [11]. However, the yield of AgNWs was lower than 72.8% regardless of the decreased diameter and high aspect ratio [5].

How to improve the yield of AgNWs, Rosa da Silva et al. reported a facile route to synthesize Ag nanowires with diameters below 20 nm and aspect ratios over 1000. The synthesis was conducted under ambient atmosphere. More importantly, the AgNW purity was as high as 85% [12]. By refluxing air and using NaBr and AgCl as co-nucleants, Liu et al. have synthesized 30-nm AgNWs with a high yield of 90% [13]. Although many preparations were carried out in ambient atmosphere, the reaction conditions were different. Some were in a bottle (disposable vial) or a three-neck flask either capped [14, 15], opened [11, 16], or refluxed [17] and it lead to different concentrations of oxygen. Some were in an autoclave reactor with different volume ratios of solution to container, neglecting the effect of air in the rest of the space [18–20]. So, the amount of oxygen was not controlled well so far and it should be optimized.

It knows that small-sized Ag nanoparticles (composed of MTPs growing into nanowires and AgNPs not growing into nanowires) are highly susceptible to oxidative etching by oxygen from atmospheric air as well as the reaction solution. The dissolved Ag nanoparticles by etching will supplement the concentration of Ag^+ ions in the solution for the growth of AgNWs, resulting in high yield of NWs [21, 22]. Oxygen-related competition between Ag nanoparticle growth and etching will determine the final morphology of AgNWs. Therefore, to obtain high-

quality AgNWs, two issues should be solved: (1) surviving small-sized MTPs and (2) etching Ag nanoparticles to grow longer AgNWs, which are both related with the oxygen content.

In this contribution, we reported a modified polyol method to prepare 91% yield AgNWs with thin diameter below 30 nm and high aspect ratio of 2500. Ag decahedral twinned seeds (MTPs) and AgNPs were incubated during the heating process from 120 to 170 °C and AgNWs were lengthened in the growth period at 170 °C. In both progresses, oxygen in the solution are controlled by different bubble gas (N_2 , Air, and O_2) and air reflux (yes or not). It is found that N_2 plays a role in the formation of MTPs with small size in the incubation. In the following growth, appropriate content of oxygen induces a long and high-yield AgNWs due to a suitable oxidative etching. The separation of incubation and growth in different atmospheres are studied for the first time. The technique has large potential for mass production of thin AgNWs with high aspect ratio and high purity.

2 Experimental

2.1 Synthesis of silver nanowires

All chemicals including silver nitrate (AgNO_3 , 99.8%), ethylene glycol (EG, 99.5%), sodium chloride (NaCl , 99.5%), sodium bromide (NaBr , 99.0%), and poly(vinyl pyrrolidone) (PVP, MW ~ 1. 300,000) were purchased from Shanghai Chemical Reagent Company and were used as received without further purification. AgNWs were synthesized by the polyol process [23]. In a standard synthesis, 0.25-g AgNO_3 were dissolved in 10-mL EG in advance. 120/60- μL NaCl/NaBr additives in EG (both 300 mM) were added into the AgNO_3 solution. After 20-min stirring, PVP (0.6 g dissolved in 20-mL EG) was poured into the mixture. The mixture in a beaker was stirred for another 20 min. After that, N_2 , air, or O_2 was bubbled in the mixed solution for 30 min in order to explore the role of oxygen. The mixture was transferred to a two-neck flask and heated at 120 °C for 10 min under magnetic stirring in an oil bath. At the same time, the flask was capped or fixed with a condenser. The mixture was then heated to 170 °C with stirring within 17 min for the incubation process. When the temperature just reached 170 °C (labeled as 0 min for the beginning of AgNW growth), N_2 or air was

Table 1 Different reaction atmospheres in the incubation from 120 to 170 °C and in the growth period at 170 °C

Sample nos	Bubble gas	Incubation	MTP size (nm)	Growth	Diameter (nm)	Aspect ratio	Yield (%)
1	O ₂	Air flux	20.8 ± 9.4	Air flux	46.2 ± 6.2	1100	80
2	Air	Air flux	13.2 ± 6.0	Air flux	38.2 ± 4.4	2000	85
3	N ₂	Capped	9.9 ± 3.6	N ₂ flux	30.1 ± 3.6	1500	72
4	N ₂	Capped	10.3 ± 4.0	Air flux	28.5 ± 3.4	2500	91

The size of MTPs (170 °C, 0 min) and parameters of AgNWs (170 °C, 30 min) are summarized

refluxed for the growth period. The reaction was kept at 170 °C without stirring and continued for 60 min to complete the synthesis. The detailed conditions, including types of bubbled gas, N₂, or air atmosphere in the incubation and growth process are summarized in Table 1. During the course of reaction, a small amount of mixture was sampled by a pipette or a syringe needle at different moments. The products were washed with ethanol and centrifuged at a high speed of 6000 rpm for 15 min three times. The final precipitates were stored in ethanol prior to microstructural and optical characterization.

2.2 Measurements

Crystal microstructures and components of Ag products were investigated by X-ray diffraction (XRD, DX-2700B) and X-ray photoelectron spectroscopy (XPS, AXIS Supra). The XPS binding energy scale was corrected with reference to the C 1s level fixed at 284.8 eV. The morphology of samples were determined by scanning electron microscopy (SEM, JSM-5900) and transmission electron microscopy (TEM, JEM 2010 UHR). The distribution of MTP size was obtained from the TEM images. The distribution of diameter and length as well as the yield of AgNWs was calculated from the SEM images. The ultraviolet-visible (UV-Vis) absorption spectra of AgNWs in ethanol and conductive films on glass were taken on a Perkin-Elmer Lambda 35 spectrometer. The sheet resistances of AgNW TCFs were measured using a four-point probe (ST2263, Suzhou Jingge).

3 Results and discussion

3.1 Nitrogen-induced small-sized MTPs retained in the incubation

Figure 1 shows digital images of AgNWs synthesized with three different atmospheres. A blue–purple

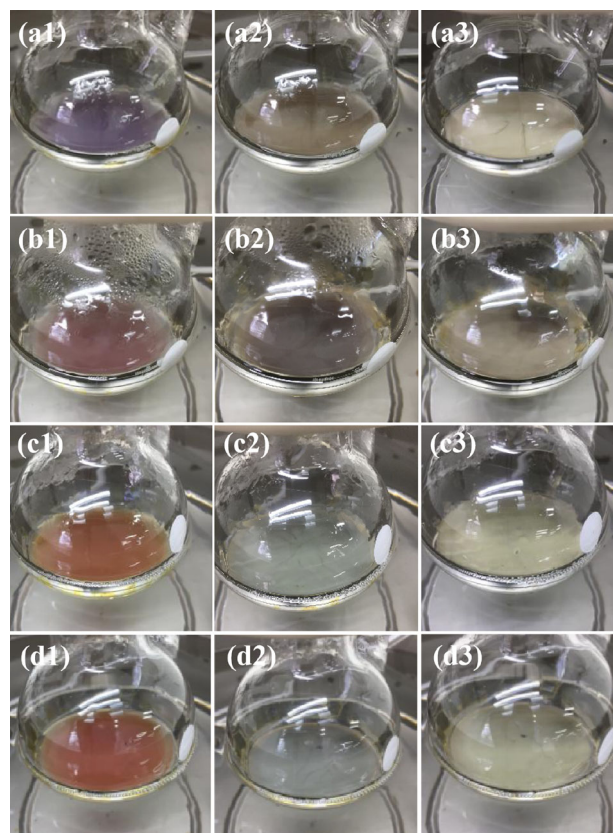


Fig. 1 Color of solution synthesized with different atmospheres for sample 1 (a1–a3), 2 (b1–b3), 3 (c1–c3), and 4 (d1–d3), at three growth stages of 0 (left), 10 (middle), and 30 min (right column) (Color figure online)

color appears in the O₂-bubbled solution (sample 1) at the beginning of growth period ($t = 0$ min), followed by a color of gray and gray–white at 10 and 30 min, respectively. In comparison, for the N₂-bubbled sample (sample 3), the solution is red–orange at 0 min. It changes from gray–green to green with the growth time increasing from 10 to 30 min. This green color is a striking feature of AgNWs with a diameter smaller than 30 nm [7, 8]. While for the reaction with ambient atmosphere (Air, sample 2), a different color of purple is observed at 0 min, as shown in Fig. 1b1.

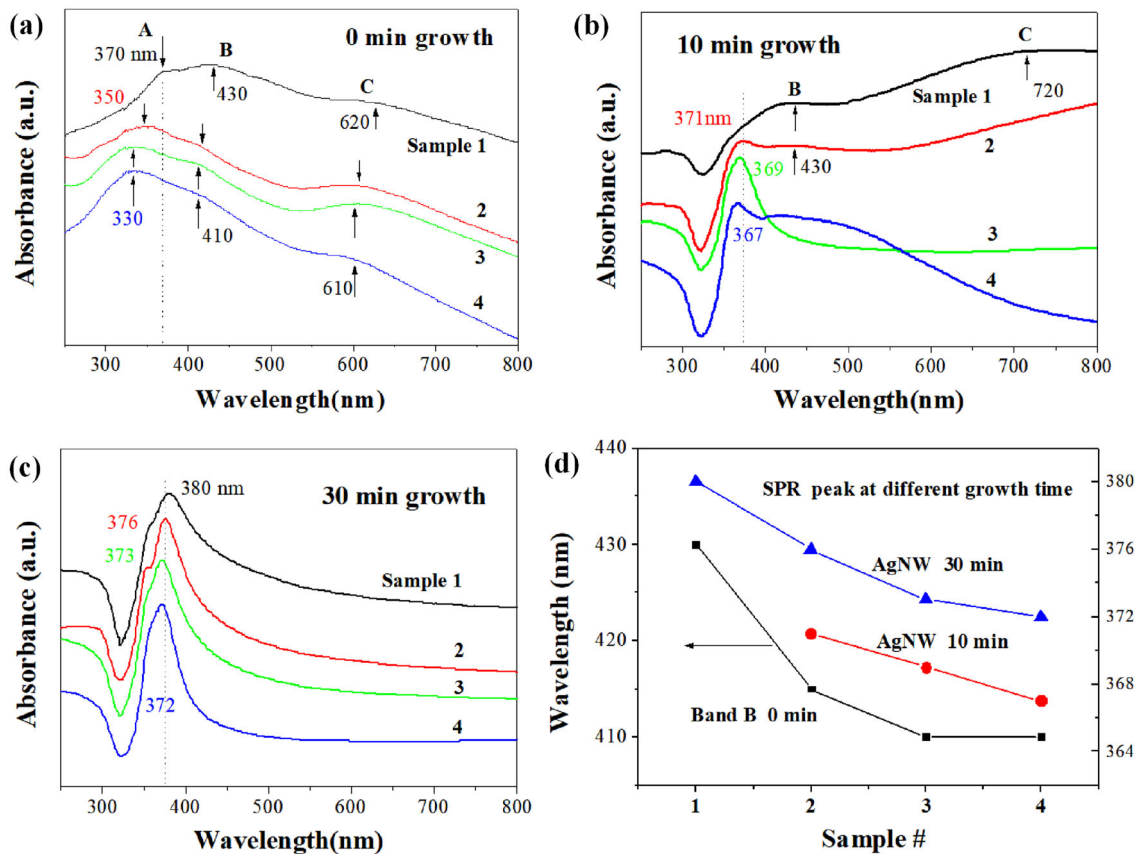


Fig. 2 Absorption spectra of samples at growth times of 0 (a), 10 (b), 30 min (c), and the corresponding SPR peaks of AgNPs and AgNWs shown in d.

This color evolves into brown and gray in the growth time of 10 and 30 min, respectively. It is indicated that synthesis with different reaction atmospheres will greatly influence the morphology of products, from which various colors appeared [11, 16, 24, 25].

The growth process of silver nanostructures was investigated in detail by UV-Vis absorption spectroscopy due to the localized surface plasmon resonance (SPR) [24, 25]. Figure 2a shows the absorption spectra of 0-min growth samples, from which three bands are observed. One is the absorption of $\text{AgBr}_{1-x}\text{Cl}_x$ crystal (330–370 nm) (band A) [26, 27] and others of 410–430 (band B) and 610–620 nm (band C) are attributed to SPR of Ag nanoparticle and transverse mode of Ag nanorod with low aspect ratio, respectively [25, 28, 29]. In addition, the SPR peak of Ag nanoparticles (band B) is red shifted from 410 to 430 nm for N_2 (sample 3 and 4)- and O_2 (sample 1)-bubbled samples, respectively, which is plotted in Fig. 2d. When the growth time is 10 min, transverse AgNW SPR peaks of 367–371 nm appear in N_2 - and

air-bubbled samples, as shown in Fig. 2b. While in the O_2 -bubbled sample (sample 1), Ag nanoparticles are the main product. For 30-min grown samples (Fig. 2c), SPR peaks are shifted to 372–380 nm. These SPR peaks are also displayed in Fig. 2d. As it is known that the position of SPR peak is sensitive to the diameter of AgNWs [9, 25]. Larger SPR position means thicker AgNWs. AgNW becomes thicker with the growth time. It is interesting to find that under the condition of N_2 protection (samples 3 and 4) thin AgNWs could be obtained.

At the same time, SEM images directly present the silver products, as shown in Fig. 3. For sample 1, large-sized MTPs and AgNPs were observed on the surface of the $\text{AgBr}_{1-x}\text{Cl}_x$ crystal at the end of incubation (0 min), as shown in Fig. 3a1 [17, 30]. However, few of them were survived and grown into AgNWs at the growth time of 10 min (Fig. 3a2). When the growth time is increased to 30 min, thick AgNWs with a mean diameter of about 46.2 nm were obtained. In contrast, small-sized MTPs and AgNPs

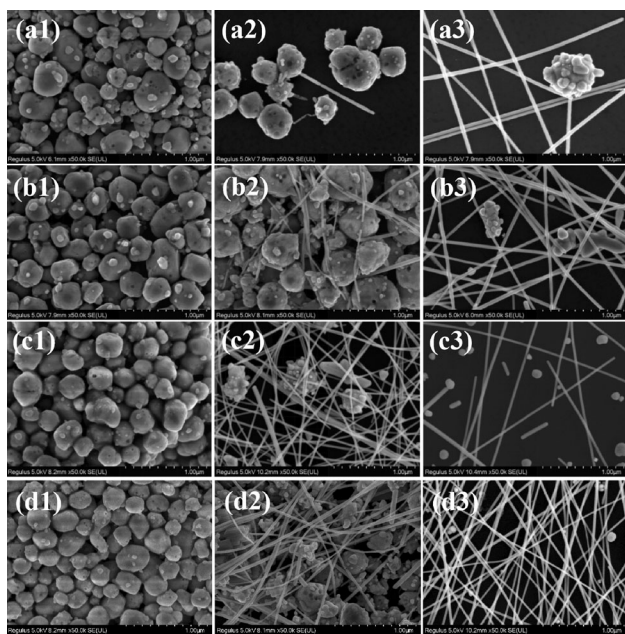


Fig. 3 SEM images of AgNWs synthesized with different atmospheres for sample 1 (a1–a3), 2 (b1–b3), 3 (c1–c3), and 4 (d1–d3) at three growth stages of 0 (left), 10 (middle), and 30 min (right column)

existed at 0 min, many of which could be grown into AgNWs at 10 min for Air- and N₂-bubbled samples, especially for the N₂-bubbled one, as shown in Fig. 3c2, d2. At 30 min, as a result, thin AgNWs with 38.2 and 30.1 nm in diameter were produced for the Air and N₂ sample, respectively. These AgNW parameters, including diameter and aspect ratio, are listed in Table 1. The low-magnified SEM images are shown in Fig. S1 (in Supporting Information), from which the distribution of diameter and length of AgNWs are calculated. The fact of increasing diameter presented in SEM images is a clear proof for the red shift of AgNW SPR peak, as shown in Fig. 2.

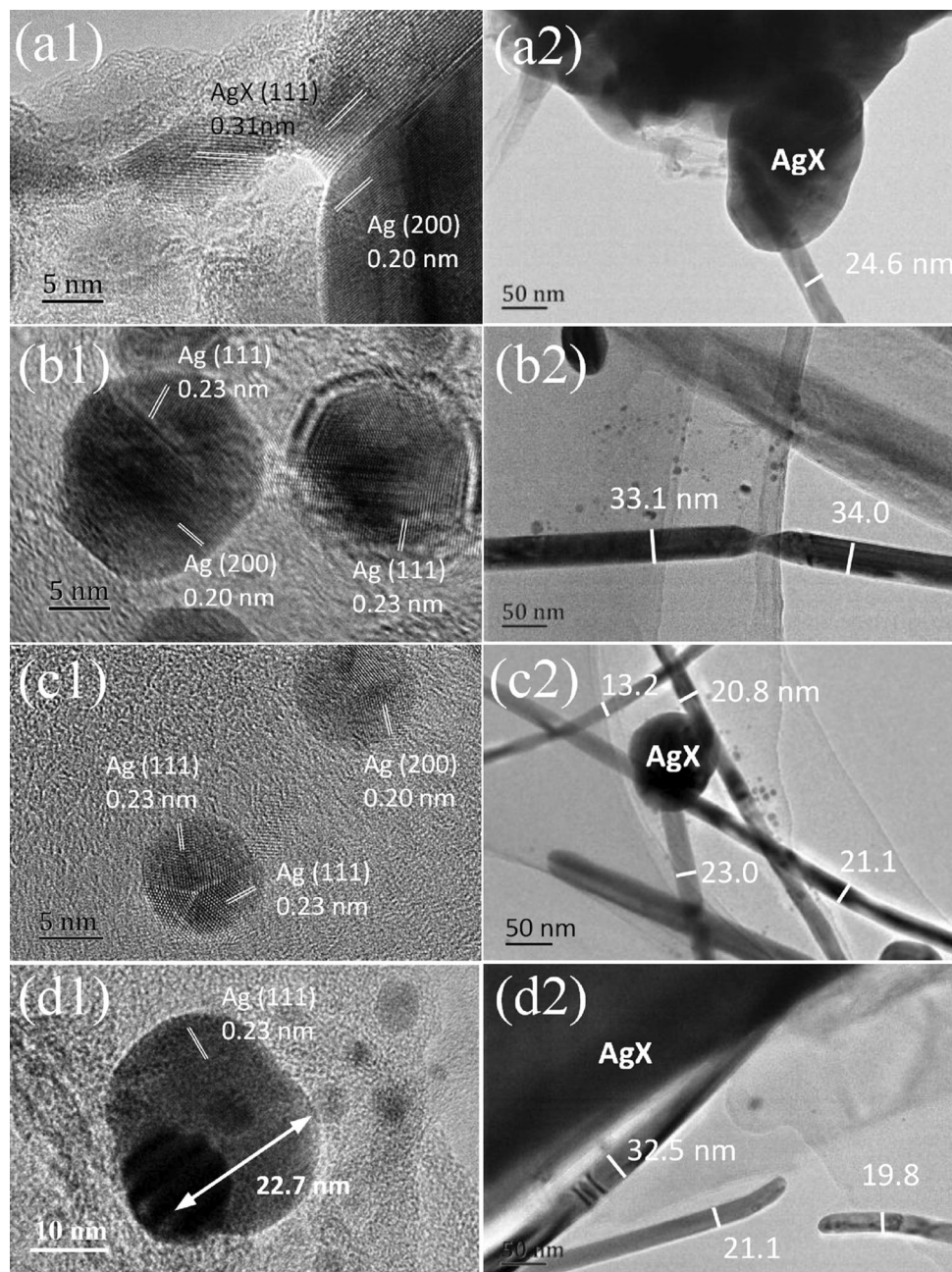
Why N₂ protection (in the incubation process from 120 to 170 °C) could synthesize AgNWs with a small diameter at last? TEM characterization is performed as shown in Fig. 4. For the 0-min grown sample (the end of incubation), Ag nanoparticles (including AgNPs and MTPs) are formed. Some AgNPs aggregate to form large-sized nanoparticles, while MTPs will grow into nanorods (Fig. 4d1) and then nanowires (Fig. 4a2–d2) [17, 23, 30]. The heterogeneous nucleant (Ag nanoparticles formed on the surface of AgX crystal) is validated, as shown in Fig. 4a1. Two contrasting components with *d*-spacing value of 0.31 and 0.20 nm are observed, respectively, which could be assigned to AgX (111) and Ag(200) planes,

respectively [31]. With the continuous reduction and dissolution, AgX crystal will be consumed. As a result, the heterogeneous nucleant Ag nanoparticles were left in the solution. With regard to MTPs, Fig. 4b1 and c1 shows their decahedral shapes and pentagonal cross facets with twin boundaries [12]. The Ag(111) and Ag(200) *d*-spacings of 0.23 and 0.20 nm are labeled by double parallel lines. The mean size (at the end of incubation) of MTPs obtained from TEM images is also listed in Table 1. It is found that MTPs with smaller size is achieved for N₂-bubbled samples (samples 3 and 4) and therefore lead to thinner AgNWs at 10-min growth time (Fig. 4c2, d2).

It knows that AgNWs will grow thicker due to the lateral deposition of Ag atoms regardless of the chemical stable Ag(100) facets packed with units of PVP [12]. Just because of the small-sized MTPs formed and retained in the N₂ protection from 120 to 170 °C, many thin AgNWs could be obtained in the 10-min growth samples, as shown in Fig. 4c2 and d2. While for the O₂-bubbled sample, due to the oxidative etching, only large-sized MTPs survive and, therefore, few thick AgNWs are generated, as presented in Fig. 4a2. Because short nanorods exist among the Ag nanoparticles for the 0-min growth sample (Fig. 4d1), this moment is called the separating point of nucleation and growth of AgNWs. Therefore, the peak of 410 nm is a characteristic peak for the start of AgNW growth [12, 25, 28]. N₂ protection in the reaction is beneficial for the formation of small-sized AgNPs and MTPs (~ 10 nm).

XPS analysis was also applied to characterize the chemical information (elemental composition, chemical status, and Ag⁰ content) of the products at the end of incubation [32, 33]. Figure 5 shows the Ag 3d XPS spectra for three samples. The Ag 3d_{5/2} and Ag 3d_{3/2} peaks can be deconvoluted into two components, in which the components at 367.3 and 373.3 eV are assigned to Ag⁺ in AgBr_{1-x}Cl_x crystal, while those at 368.1 and 374.0 eV belong to Ag⁰. The XPS result confirmed the presence of Ag⁰ in the AgBr_{1-x}Cl_x crystal. Based on the peak areas in XPS, the surface content ratio of metallic Ag⁰ in the total Ag were calculated to be 7.6, 8.7, and 10.2 at.% for the N₂-, Air-, and O₂-bubbled samples, respectively. The increased content of Ag⁰ demonstrates that oxygen is helpful to the reduction of Ag⁺ due to glycolaldehyde (GA) production [34]. Therefore, large-sized Ag nanoparticles were formed in sample 1. However,

Fig. 4 TEM images of samples 1–4 at the end of incubation (left) and 10 growth time (right column)



also due to oxidative etching, only large-sized MTPs survived, as shown in Fig. 4a1. For the N_2 -bubbled one (samples 3 and 4), because of the lack of oxidative etching, small-sized Ag MTPs could be produced and retained.

On the other hand, Fig. 5 also shows that the total Ag content (Ag^0 and Ag^+) in $AgBr_{1-x}Cl_x$ crystal is decreased to 59.1 at.% for the O_2 sample. Once Ag nanoparticles on the surface of $AgBr_{1-x}Cl_x$ crystal are dissolved to Ag^+ ions, they are preferentially bonded with Br^- because the redox potential of + 0.223 V for

$AgCl/Ag$ pair is higher than that of + 0.007 V ($AgBr/Ag$ pair) [33, 35]. As a result, contents of Cl and Br increase with oxygen content, as shown in Fig. S2 in Supporting Information. The Br/Cl ratio is increased from 0.404 to 0.417 for the N_2 (sample 3)- and O_2 (sample 1)-bubbled sample, respectively. Therefore, the higher Br/Cl ratio is the evidence of oxidative etching and dissolution of AgNPs, providing more possibility for the formation of $AgBr_{1-x}Cl_x$ crystal with higher Br content. It is evident that the absorption band was red shifted from 330 nm for N_2 -

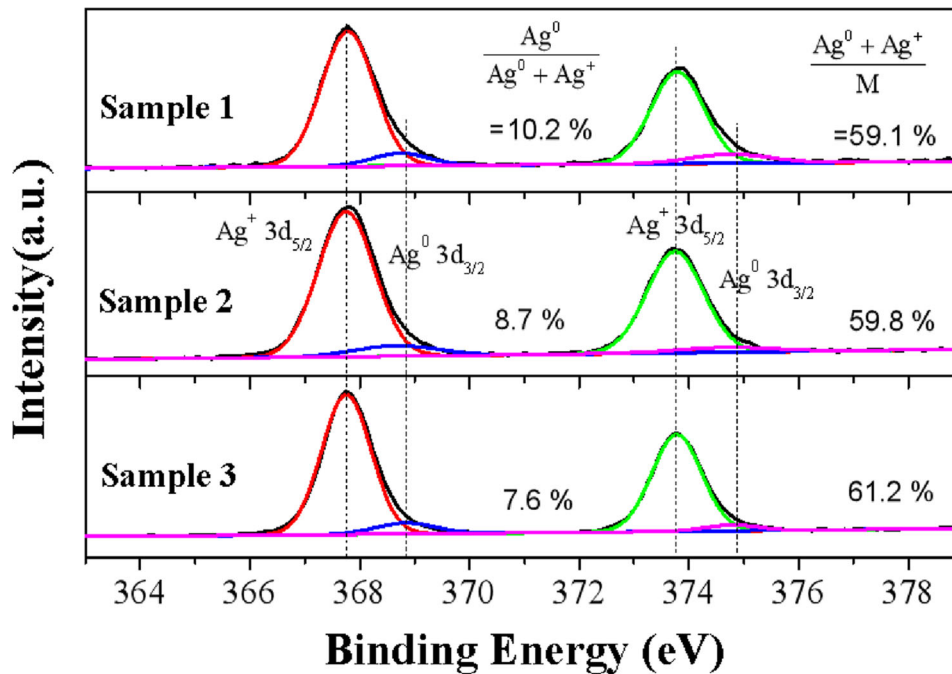


Fig. 5 XPS spectra of samples at the end of incubation with the atomic concentration of Ag (including Ag⁰ and Ag⁺) labeled. $M = \text{Ag}(3d) + \text{Cl}(2p) + \text{Br}(3d)$

bubbled sample (sample 3 with a red–orange color) to 370 nm for the O₂-bubbled sample (sample 1 with a blue–purple color), as shown in Fig. 2a.

3.2 Oxygen etching for high yield in the growth

For the growth period, N₂ or Air was fluxed. It is found that air flux is in favor of high yield of AgNWs. As displayed in SEM images, the higher yields of 80 and 85% were obtained for samples 1 and 2, compared with that (72%) for sample 3 with N₂ reflux. When the sample was protected in N₂ (incubation) and refluxed with air (growth), a higher AgNW yield of 91% was obtained.

XRD was applied to investigate the evolution of silver nanostructures, as shown in Fig. 6. At the beginning of growth, no Ag signal was detected for all samples. Although Ag nanoparticles were formed (shown in TEM images, SPR band in absorption spectra, and XPS result), the percentage of Ag nanoparticles was not high and only peaks of AgBr_{1-x}Cl_x crystal appeared. At 10 min, Ag(111) and Ag(200) peaks were clearly observed for the N₂ sample, whose intensity was decreased with the oxygen content, as shown with arrows in the dotted rectangle of Fig. 6. Due to oxidative etching and

dissolution of MTPs and AgNPs, Ag signal was weak in sample 1. Therefore, few MTPs with large sizes survived and were grown into AgNWs with a thick diameter, as shown in Fig. 3a2. In addition, many holes were left on the surface of AgBr_{1-x}Cl_x crystal, which indicates that Ag nanoparticles have separated from them due to etching of oxygen (Fig. 3a2) [25]. On the other hand, the diffraction angle of AgBr_{1-x}Cl_x(220) was decreased from 45.3 to 45.1 for the N₂ and O₂ samples, respectively, when the growth time is 0 min. This decrease is originated from the larger lattice constant of AgBr_{1-x}Cl_x crystal. Because of oxidative etching, more Br⁻ ions are incorporated into the AgCl lattice, resulting in the formation of AgBr_{1-x}Cl_x crystal with higher Br content, which is in agreement with the XPS results [27].

After 30-min growth, AgBr_{1-x}Cl_x crystal are completely consumed and only AgNWs and AgNPs exist in each sample. Due to the enrichment of (111) planes of AgNWs, the ratio of Ag(111)/Ag(200) intensity acts as an indicator for the aspect ratio of AgNWs [36]. Each ratio is presented in the diffraction spectra in Fig. 6. It is found that an intensity ratio of 6.5 and 7.1 were obtained for samples 3 and 4, respectively. These two samples were both bubbled by N₂ and capped in incubation, but undergo different

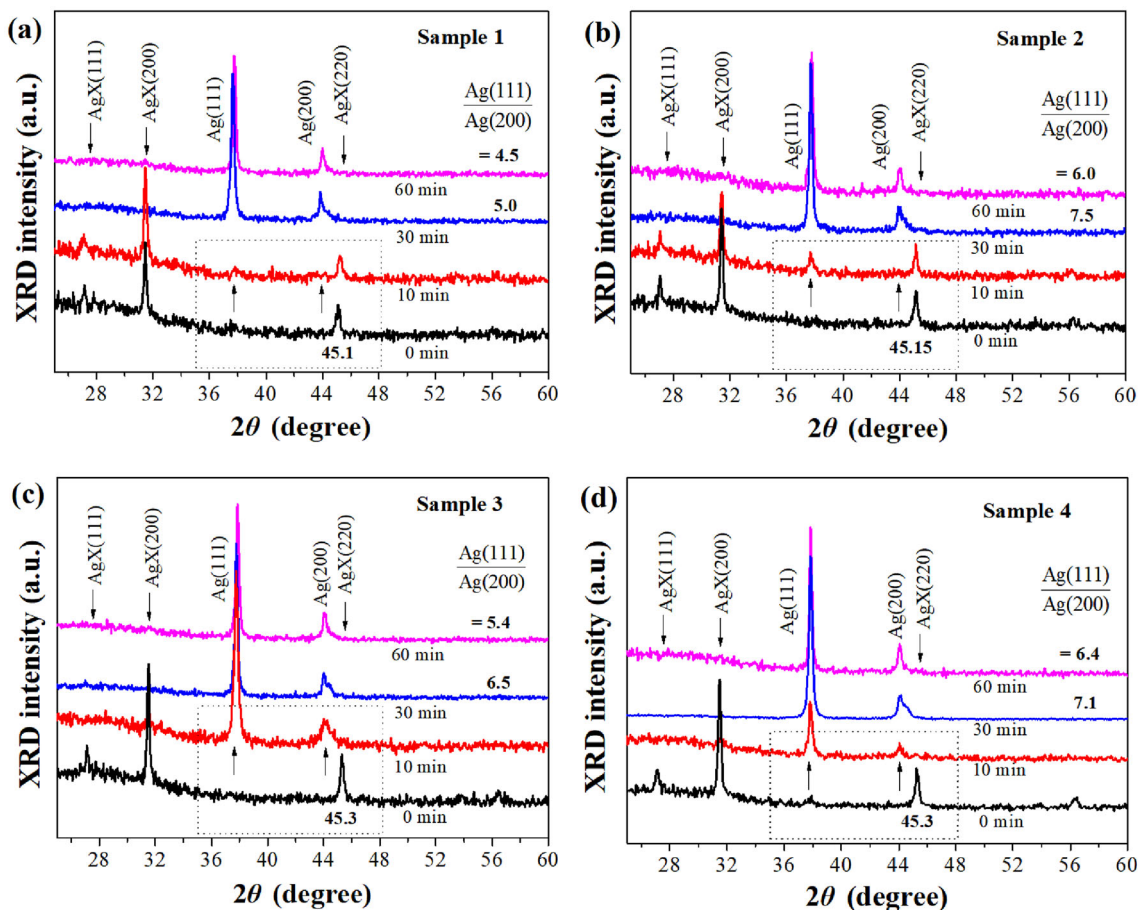


Fig. 6 XRD pattern of AgNWs prepared for sample 1 (a), 2 (b), 3 (c), and 4 (d). Diffraction peaks of metallic Ag and crystal of AgX ($X = Br_{1-x}Cl_x$) are labeled and the intensity ratio of Ag(111)/Ag(200) is presented in each XRD pattern

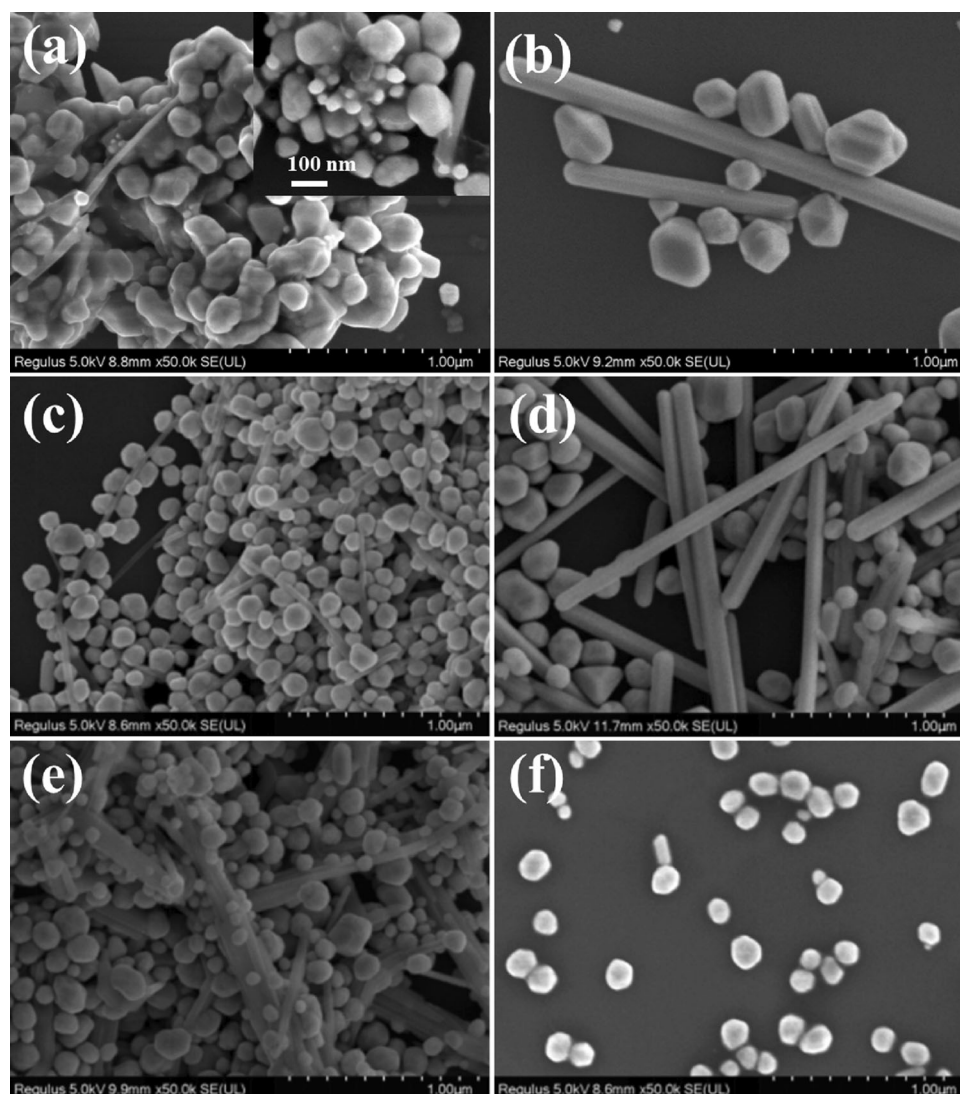
atmosphere reflux in growth period. Oxidative etching of AgNPs leads to a higher intensity ratio (7.1) of Ag(111)/Ag(200) and as a result, a higher aspect ratio of 2500 for sample 4 was obtained.

To explore the role of oxygen more clearly, a control experiment was carried out *without halide ions* (Cl^- or Br^-), as shown in Fig. 7. For the N_2 -refluxed sample, only Ag nanoparticles were obtained with an unchanged size (~ 80 nm) from 10 to 30 min. While in Air sample, besides big Ag nanoparticles (~ 100 nm), several AgNWs were produced at the growth time of 30 min, as shown in Fig. 7d. When the solution is bubbled with O_2 and refluxed in air, bigger-sized Ag nanoparticles (~ 200 nm) and thick AgNWs (150 nm in diameter) are both produced. Interestingly, some Ag nanoparticles stick to each other and fuse together for the O_2 sample (Fig. 7a),

instead of separating each other for the N_2 sample (Fig. 7e), which is the evidence of oxidative etching effect. The remarkable etching lets small Ag nanoparticles dissolve and coalesce with bigger particles via the Ostwald ripening process [29, 37]. So, the boundary of each Ag nanoparticle disappears. Small Ag nanoparticles with a size of 25 nm was observed in the growth stage of 10 min, as shown in the inset of Fig. 7a. While in the N_2 and Air samples, Ag nanoparticles are individuals as oxidative etching is weak. Therefore, etching is beneficial to make AgNWs grow longer.

In addition, several “tender nanowires” are emerged among Ag nanoparticles, as shown in Fig. 7c and e. However, these “tender nanowires” could not grow into AgNWs. They are composed of many small Ag nanoparticles wrapped with

Fig. 7 SEM images of AgNWs synthesized **without any additives**, but the same reaction atmosphere as sample 1 (a, b), 2 (c, d), and 3 (e, f) at the growth time of 10 (left) and 30 min (right column)

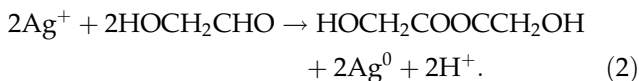
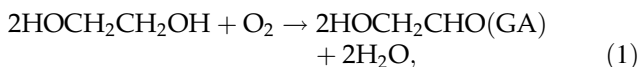


amorphous PVP, most of which are MTPs with a mean size of 11.0 nm, as shown in Fig. 8a. In comparison, Fig. 8b gives the TEM image of a single AgNW. The lattice spacings of 0.24 and 0.20 nm for Ag(111) and Ag(200), respectively, are marked in Fig. 8. From the SAED pattern given in the inset of Fig. 8a, several sets of spots are displayed, which indicate the discrete MTPs in the “tender nanowires.” In contrast, only two sets of SAED patterns (inset of Fig. 8b) are detected in the AgNW sample due to the bicrystalline structure with the [110] growth direction. A large lattice spacing of 0.38 nm is related with the superimposition of upper and lower single subunits of this five-fold-twinned AgNW [38]. So in the sample with N_2 bubble and N_2 reflux, MTPs in the “tender nanowires” will individually grow into Ag

nanoparticles rather than AgNWs, due to the lack of oxidative etching.

3.3 Mechanism of separation between nucleation and growth

Figure 9 shows the schematic illustration describing the role of oxygen in the polyol synthesis of AgNWs. The ellipse presents the crystal of $AgBr_{1-x}Cl_x$. In the incubation process, MTPs (pentagon) and AgNPs (circle) were formed on the surface of $AgBr_{1-x}Cl_x$ crystals due to the reductant GA, whose size and amount are controlled by the concentration of oxygen [16, 34, 39]. Oxygen is needed to improve the oxidation of EG to GA. GA will reduce Ag^+ to the atomic Ag and then form Ag nanoparticles.



At the same time, due to the oxidative etching, oxygen will also etch the formed Ag nanoparticles and dissolve them.



Therefore, the concentration of oxygen has to be well controlled and more O_2 , higher density, and large-sized nanoparticles will be obtained. However, the remarkable oxygen in the solution will etch and dissolve small nanoparticles and then gather into bigger particles. Therefore, a small number of large-sized MTPs and AgNPs were retained, as shown in Fig. 9a. With the same reason, only large-sized MTPs will grow into AgNWs with thick diameters. In contrast, due to the lack of oxygen for N_2 samples (samples 3 and 4), the production of GA is suppressed and etching of oxygen is limited. So, small-sized MTPs and AgNPs were formed and preserved. As presented by TEM and SEM images, a large number of small Ag nanoparticles (MTPs and AgNPs) exist on the surface of $\text{AgBr}_{1-x}\text{Cl}_x$ crystals, as shown in Fig. 9g and j. The air sample has moderate concentration of oxygen, which is a benefit for middle-sized AgNPs. Therefore, MTPs with decreased size can be obtained by reducing content of oxygen.

While for the growth period, suitable oxygen is critical for the high-yield growth of AgNWs with thin diameter. When oxidative etching happens, Ag nanoparticles will be dissolved into Ag^+ ions, which,

in turn, act as the source of the growth of AgNWs. In sample 3, the concentration of Ag^+ in the solution is low due to the lack of oxidative etching. The limited Ag^0 will be only preferentially deposited on the (111) facet, which is presented by an arrow in Fig. 9h. Although thin AgNWs (30.1 nm) were obtained, large number of AgNPs (72% AgNW yield in our case) were remained in the N_2 -refluxed sample (Fig. 9i). By increasing oxygen content by refluxing in air during the growth period, the yield of AgNWs was improved due to oxidative etching and Ag^+ supply in the solution. Two arrows are depicted in Fig. 9e, indicating the elongation as well as the lateral growth of AgNWs for a higher yield of AgNWs (Fig. 9f, l). For the O_2 -bubbled and air reflux sample (sample 1), the etching of oxygen is remarkable and it resulted in sufficient Ag^+ ions in the solution. Adequate Ag^0 was produced and deposited itself on the (111) and (100) facets, as shown by three arrows in Fig. 9b. So thick AgNWs (46.2 nm) were obtained, but a lower yield of 80% for AgNWs was reached in sample 1. It is similar that excessive Fe^{3+} and Cu^{2+} will produce other nanostructure besides AgNWs because of the strong etching effect [9, 12, 20, 40]. Therefore, the etchants, such as O_2 and $\text{Fe}^{3+}(\text{Cu}^{2+})$, should have appropriate concentrations for the high-yield synthesis of AgNWs.

In our case, sample 4 was bubbled with N_2 and capped in the incubation, and many MTPs and AgNPs of small sizes (~ 10 nm with a SPR peak of 410 nm) could be generated on the surface of $\text{AgBr}_{1-x}\text{Cl}_x$ crystals. In the growth process, for a suitable oxidative etching, appropriate oxygen was applied by ambient atmosphere reflux. As a result, AgNWs are grown along the $\langle 110 \rangle$ direction, while the lateral growth is somewhat restrained. Therefore, by controlling the concentration of oxygen, the MTP formation in the incubation and AgNW elongation in the growth period are well separated, which leads to a higher AgNW yield of 91%, as shown in Fig. 3d3. In combination with the diameter of 28.5 nm and aspect ratio of 2500, our AgNWs have a higher quality than those in other reports, as summarized in Table S1 in Supporting Information. Dan Jia et al. reported a synthetic method for AgNWs (20 nm diameter) with a very high yield of 94.5%. High temperature of 180 °C was applied to nucleate homogeneously and heterogeneously, while the growth of AgNWs was conducted at 160 °C. The lower growth temperature is helpful to suppress secondary homogeneous

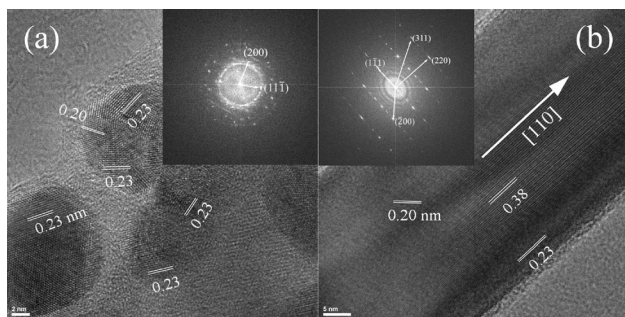


Fig. 8 TEM images and the SAED pattern (inset) of a “tender nanowire” (a) and a single AgNW (b) produced at 10-min growth for sample similar to samples 3 and 1, respectively, but synthesized without any additives

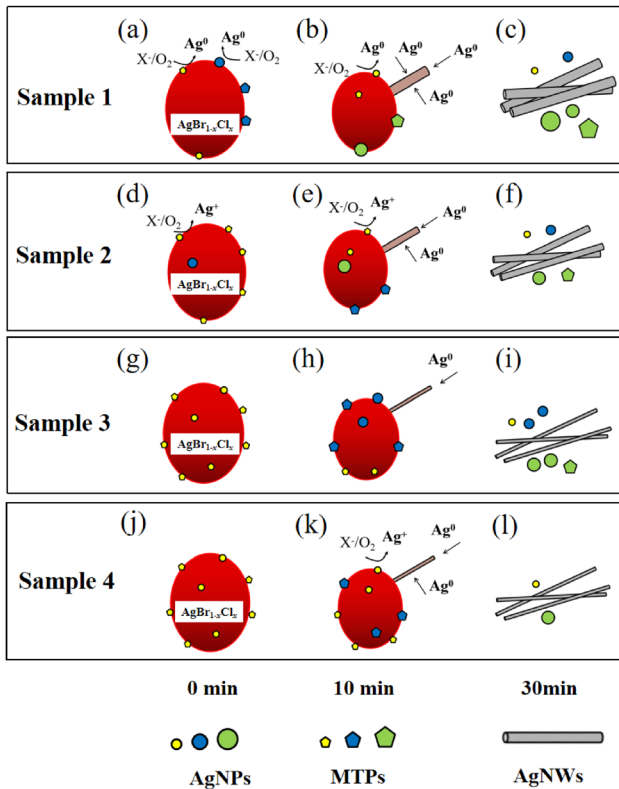


Fig. 9 A schematic illustration depicting oxygen-induced separation of nucleation and growth in the AgNW polyol synthesis for sample 1 (a–c), 2 (d–f), 3 (g–i), and 4 (j–l) at three growth stages of 0 (left), 10 (middle) and 30 min (right column). N₂ is beneficial for the formation of small-sized MTPs and AgNPs at the end of incubation (g, j). While in the growth period, O₂ and Air will etch and dissolve AgNPs for high-yield AgNWs (f, l)

seeding [5]. We believe that this strategy of high and low temperature can play the role of separating nucleation and growth for AgNW synthesis with high purity, similar to that in our case.

3.4 Properties of TCFs

Finally, TCFs were prepared by the method described in our previous work [23]. Some air-dried films were annealed in an oven for 20 min in air at different temperatures. Figure 10a shows optical transmittance spectra of TCFs dried in air at room temperature. The highest *T* of 97.0% was obtained in sample 4. When samples were annealed at an increasing temperature, *T* changed very small, while the sheet resistance (*R_s*) reduced significantly, as

shown in Fig. 10c and d, respectively. All samples present a low *R_s* and high *T* at the annealing temperature of 140 °C, satisfying the minimum standard (“doorsill” of *R_s* ≤ 100 Ω/sq when *T* = 90%) for industrial production of TCFs [25]. When the annealing temperature was increased to 200 °C, *R_s* was increased due to the junction breaking of the AgNWs [41].

H. Kang et al. have studied electrical properties for AgNW network electrode. *R_s* was reduced because of the thermal welding among Ag nanowires at each junction. The welding process induces subtle movements of AgNWs on nano/microscale but does not change the area ratio of the nanowires [42, 43]. As a result, optical transmittance is preserved during the heating treatment. Therefore, thin and high aspect AgNWs are desired for TCFs because thin nanowires scatter less light and the high aspect ratio decreases the number of nanowire–nanowire contacts in the film [6]. As diameter decreases, the transmittance is increased for a given resistance. In our case, due to the small diameter of 28.5 nm and aspect ratio of 2500 in sample 4, the performance of *T* = 97.0% and *R_s* = 48 Ω/sq was obtained, which is superior to the commercial ITO [7]. The comparable *T* and *R_s* reported by others is also given in Table S1 (in Supporting Information).

4 Conclusion

In summary, we have developed a facile method to produce thin AgNWs (~ 28 nm) with a high yield of 91% by separating nucleation and growth. This separation was realized through different concentrations of oxygen during the synthesis. Small-sized MTPs and AgNPs were formed and retained under N₂ bubble and N₂ protection in the incubation process. While for the growth period, suitable oxygen is adopted to etch AgNPs and produce high-yield AgNWs with a high aspect ratio. TCFs prepared with this high-quality AgNWs in our case have an excellent performance with sheet resistance of 48 Ω/sq and transmittance of 97.0% at 550 nm, which is promising for flexible electronic devices and touch panel applications. The precise adjustment of oxygen in the AgNW synthesis is under way in our lab.

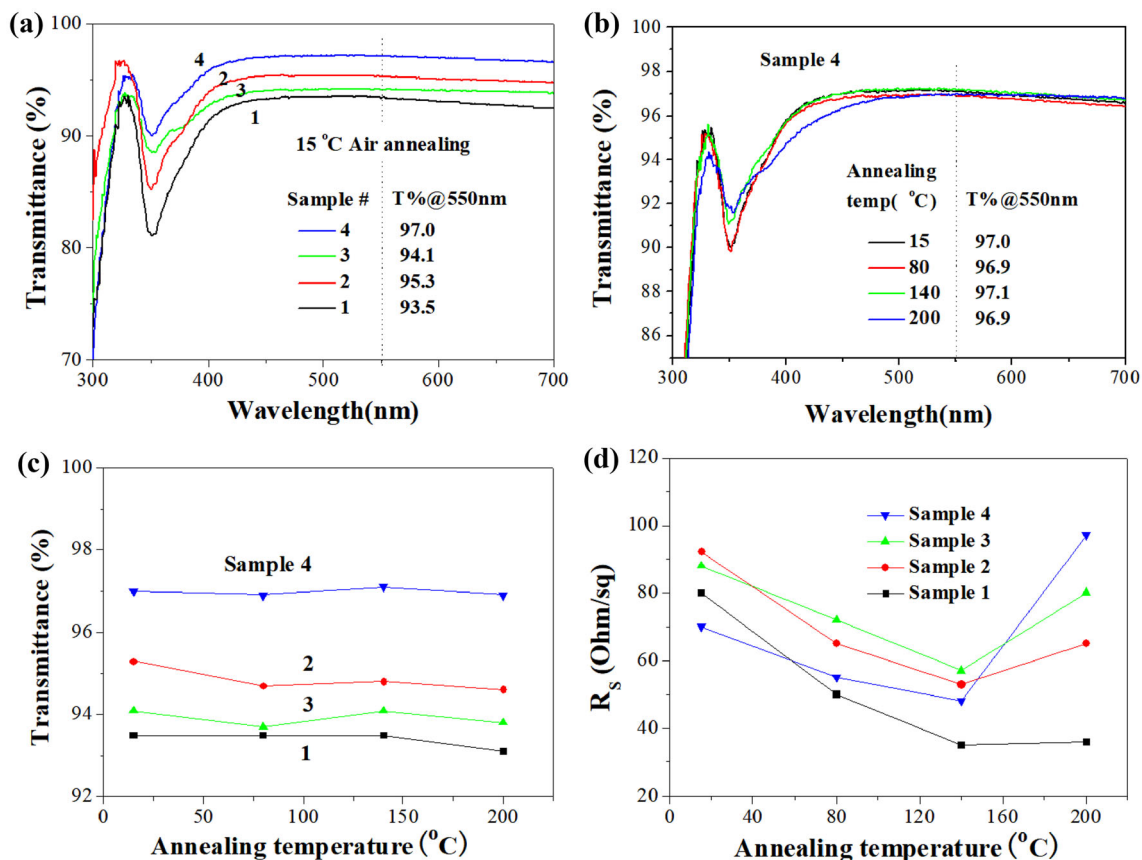


Fig. 10 Optical transmittance spectra of TCFs dried at room temperature for all samples in air (a) and heated at other annealing temperatures in air for sample 4 (b). The changes of transmittance

and sheet resistance with annealing temperatures are shown in c and d, respectively

Author contributions

YJ and RT designed and conducted the experiment and wrote the manuscript. HZ and NW carried out the UV–Vis absorption and XRD measurements and data analysis. XPS, SEM, TEM, and electrical measurements and data analysis were done by YY, DG, and TZ. YR and JX supervised the project and reviewed and edited the manuscript. All authors have approved the final version of the manuscript.

Funding

This work was supported by the National Natural Science Foundation of China (NSFC Nos. 61704079, 11674053), the Open Project of National Laboratory of Solid-State Microstructures, and the National Undergraduate Training Program for Innovation and Entrepreneurship (202110291129Z) and PAPD.

Data availability

The datasets generated and analyzed during the current study are available from the corresponding author on reasonable request.

Declarations

Conflict of interest The authors declare that they have no known competing financial interests or personal relationships that could have appeared to influence the work reported in this paper.

Supplementary Information: The online version contains supplementary material available at <http://doi.org/10.1007/s10854-022-09454-5>.

References

1. X. Zhai, W. Wang, J. Jia, P. Dong, One-step synthesis of ultra-high aspect ratio silver nanowires for high-performance

- flexible transparent conductive films. *J. Mater. Sci. Mater. Electron.* **32**, 15622–15632 (2021)
2. Y. Zhu, Y. Deng, P. Yi, L. Peng, X. Lai, Z. Lin, Flexible transparent electrodes based on silver nanowires: material synthesis, fabrication, performance, and applications. *Adv. Mater. Technol.* **4**, 1900413 (2019)
 3. W. Zhang, W. Song, J. Huang, L. Huang, T. Yan, J. Ge, R. Peng, Z. Ge, Graphene:silver nanowire composite transparent electrode based flexible organic solar cells with 13.4% efficiency. *J. Mater. Chem. A* **7**, 22021–22028 (2019)
 4. H. Sun, X. Li, Z. Hu, C. Gu, D. Chen, J. Wang, B. Li, T. Jiang, X. Zhou, Hydrophilic–hydrophobic silver nanowire-paper based SERS substrate for in situ detection of furazolidone under various environments. *Appl. Surf. Sci.* **556**, 149748 (2021)
 5. D. Jia, Y. Zhao, W. Wei, C. Chen, G. Lei, M. Wan, J. Tao, S. Li, S. Ji, C. Ye, Synthesis of very thin Ag nanowires with fewer particles by suppressing secondary seeding. *CrytEngComm* **19**, 148–153 (2017)
 6. S.M. Bergin, Y.H. Chen, A.R. Rathmell, P. Charbonneau, Z.Y. Li, B.J. Wiley, The effect of nanowire length and diameter on the properties of transparent, conducting nanowire films. *Nanoscale* **4**, 1996–2004 (2012)
 7. B. Li, S. Ye, I.E. Stewart, S. Alvarez, B.J. Wiley, Synthesis and purification of silver nanowires to make conducting films with a transmittance of 99%. *Nano Lett.* **15**, 6722–6726 (2015)
 8. K. Zhang, Y. Du, S. Chen, Sub 30 nm silver nanowire synthesized using KBr as co-nucleant through one-pot polyol method for optoelectronic applications. *Org. Electron.* **26**, 380–385 (2015)
 9. X.M. Wang, L. Chen, E. Sowade, R.D. Rodriguez, E. Sheremet, C.M. Yu, R.R. Baumann, J.J. Chen, Ultra-uniform and very thin Ag nanowires synthesized via the synergy of $\text{Cl}^{(-)}$, $\text{Br}^{(-)}$ and $\text{Fe}^{(3+)}$ for transparent conductive films. *Nanomaterials* **10**, 237 (2020)
 10. E.J. Lee, Y.H. Kim, D.K. Hwang, W.K. Choi, J.Y. Kim, Synthesis and optoelectronic characteristics of 20 nm diameter silver nanowires for highly transparent electrode films. *RSC Adv.* **6**, 11702 (2016)
 11. K.E. Korte, S.E. Skrabalak, Y. Xia, Rapid synthesis of silver nanowires through a CuCl - or CuCl_2 -mediated polyol process. *J. Mater. Chem.* **18**, 437–441 (2008)
 12. R.R. da Silva, M. Yang, S.I. Choi, M. Chi, M. Luo, C. Zhang, Z.Y. Li, P.H. Camargo, S.J. Ribeiro, Y. Xia, Facile synthesis of sub-20 nm silver nanowires through a bromide-mediated polyol method. *ACS Nano* **10**, 7892–7900 (2016)
 13. Y. Liu, Y. Chen, R. Shi, L. Cao, Z. Wang, T. Sun, J. Lin, J. Liu, W. Huang, High-yield and rapid synthesis of ultrathin silver nanowires for low-haze transparent conductors. *RSC Adv.* **7**, 4891–4895 (2017)
 14. S. Zhu, Y. Gao, B. Hu, J. Li, J. Su, Z. Fan, J. Zhou, Transferable self-welding silver nanowire network as high performance transparent flexible electrode. *Nanotechnology* **24**, 335202 (2013)
 15. S. Chang, K. Chen, Q. Hua, Y. Ma, W. Huang, Evidence for the growth mechanisms of silver nanocubes and nanowires. *J. Phys. Chem. C* **115**, 7979–7986 (2011)
 16. J. Ma, M. Zhan, Rapid production of silver nanowires based on high concentration of AgNO_3 precursor and use of FeCl_3 as reaction promoter. *RSC Adv.* **4**, 21060 (2014)
 17. W.M. Schuette, W.E. Buhro, Silver chloride as a heterogeneous nucleant for the growth of silver nanowires. *ACS Nano* **7**, 3844–3853 (2013)
 18. Y. Zhang, J. Guo, D. Xu, Y. Sun, F. Yan, One-pot synthesis and purification of ultralong silver nanowires for flexible transparent conductive electrodes. *ACS Appl. Mater. Interfaces* **9**, 25465–25473 (2017)
 19. D. Chen, X. Qiao, X. Qiu, J. Chen, R. Jiang, Large-scale synthesis of silver nanowires via a solvothermal method. *J. Mater. Sci. Mater. Electron.* **22**, 6–13 (2010)
 20. L. Zhang, F. Jiang, B. Wu, C. Lv, M. Wu, A one-step synthesis of ultra-long silver nanowires with ultra-high aspect ratio above 2000 and its application in flexible transparent conductive electrodes. *Nanotechnology* **32**, 105710 (2021)
 21. R. Long, S. Zhou, B.J. Wiley, Y. Xiong, Oxidative etching for controlled synthesis of metal nanocrystals: atomic addition and subtraction. *Chem. Soc. Rev.* **43**, 6288–6310 (2014)
 22. X. Tang, M. Tsuji, P. Jiang, M. Nishio, S.-M. Jang, S.-H. Yoon, Rapid and high-yield synthesis of silver nanowires using air-assisted polyol method with chloride ions. *Colloids Surf. A* **338**, 33–39 (2009)
 23. Y. Rui, W. Zhao, D. Zhu, H. Wang, G. Song, M.T. Swihart, N. Wan, D. Gu, X. Tang, Y. Yang, T. Zhang, Understanding the effects of NaCl , NaBr and their mixtures on silver nanowire nucleation and growth in terms of the distribution of electron traps in silver halide crystals. *Nanomaterials* **8**, 161 (2018)
 24. T. Huang, X.H. Nancy Xu, Synthesis and characterization of tunable rainbow colored colloidal silver nanoparticles using single-nanoparticle plasmonic microscopy and spectroscopy. *J. Mater. Chem.* **20**, 9867–9876 (2010)
 25. K. Zhan, R. Su, S. Bai, Z. Yu, N. Cheng, C. Wang, S. Xu, W. Liu, S. Guo, X.Z. Zhao, One-pot stirring-free synthesis of silver nanowires with tunable lengths and diameters via a $\text{Fe}^{(3+)}$ and $\text{Cl}^{(-)}$ co-mediated polyol method and their application as transparent conductive films. *Nanoscale* **8**, 18121–18133 (2016)

26. Z. Li, Y. Sun, Silver chlorobromide nanoparticles with highly pure phases: synthesis and characterization. *J. Mater. Chem. A* **1**, 6786–6793 (2013)
27. M. Zhu, C. Chen, P. Chen, B. Lei, W. Ma, M. Liu, Sunlight-driven Ag–AgCl_(1-x)Br_(x) photocatalysts: enhanced catalytic performances via continuous bandgap-tuning and morphology selection. *Phys. Chem. Chem. Phys.* **15**, 12709–12716 (2013)
28. Y. Sun, Y. Yin, B.T. Mayers, T. Herricks, Y. Xia, Uniform silver nanowires synthesis by reducing AgNO₃ with ethylene glycol in the presence of seeds and poly(vinyl pyrrolidone). *Chem. Mater.* **14**, 4736–4745 (2002)
29. C. An, J. Wang, S. Wang, Q. Zhang, M. Yang, J. Zhan, Converting AgCl nanocubes to silver nanowires through a glycerol-mediated solution route. *CrystEngComm* **14**, 5886–5891 (2012)
30. C. Wang, B. Cheng, H. Zhang, P. Wan, L. Luo, Y. Kuang, X. Sun, Probing the seeded protocol for high-concentration preparation of silver nanowires. *Nano Res.* **9**, 1532–1542 (2016)
31. S. Zhou, J. Li, K.D. Gilroy, J. Tao, C. Zhu, X. Yang, X. Sun, Y. Xia, Facile synthesis of silver nanocubes with sharp corners and edges in an aqueous solution. *ACS Nano* **10**, 9861–9870 (2016)
32. Q. Li, S. Chang, D. Wu, S. Bao, C. Zeng, M. Nasir, B. Tian, J. Zhang, Synthesis of cubic Ag@AgCl and Ag@AgBr plasmonic photocatalysts and comparison of their photocatalytic activity for degradation of methyl orange and 2,4-dichlorophenol. *Res. Chem. Intermed.* **44**, 4651–4661 (2018)
33. W. Kong, S. Wang, D. Wu, C. Chen, Y. Luo, Y. Pei, B. Tian, J. Zhang, Fabrication of 3D sponge@AgBr–AgCl/Ag and tubular photoreactor for continuous wastewater purification under sunlight irradiation. *ACS Sustain. Chem. Eng.* **7**, 14051–14063 (2019)
34. S.E. Skrabalak, B.J. Wiley, M. Kim, E.V. Formo, Y. Xia, On the polyol synthesis of silver nanostructures: glycolaldehyde as a reducing agent. *Nano Lett.* **8**, 2077–2081 (2008)
35. Y. Bi, J. Ye, Direct conversion of commercial silver foils into high aspect ratio AgBr nanowires with enhanced photocatalytic properties. *Chem. Eur. J.* **16**, 10327–10331 (2010)
36. J. Jiu, K. Murai, D. Kim, K. Kim, K. Suganuma, Preparation of Ag nanorods with high yield by polyol process. *Mater. Chem. Phys.* **114**, 333–338 (2009)
37. R. Prucek, A. Panáček, A. Fargašová, V. Ranc, V. Mašek, L. Kvítek, R. Zbořil, Re-crystallization of silver nanoparticles in a highly concentrated NaCl environment—a new substrate for surface enhanced IR–visible Raman spectroscopy. *CrystEngComm* **13**, 2242 (2011)
38. Z. Niu, F. Cui, E. Kuttner, C. Xie, H. Chen, Y. Sun, A. Dehestani, K. Schierle-Arndt, P. Yang, Synthesis of silver nanowires with reduced diameters using benzoic acid-derived radicals to make transparent conductors with high transparency and low haze. *Nano Lett.* **18**, 5329–5334 (2018)
39. H. Ding, Y. Zhang, G. Yang, S. Zhang, L. Yu, P. Zhang, Large scale preparation of silver nanowires with different diameters by a one-pot method and their application in transparent conducting films. *RSC Adv.* **6**, 8096–8102 (2016)
40. A. Taguchi, S. Fujii, T. Ichimura, P. Verma, Y. Inouye, S. Kawata, Oxygen-assisted shape control in polyol synthesis of silver nanocrystals. *Chem. Phys. Lett.* **462**, 92–95 (2008)
41. S. Coskun, E.S. Ates, H.E. Unalan, Optimization of silver nanowire networks for polymer light emitting diode electrodes. *Nanotechnology* **24**, 125202 (2013)
42. H. Kang, Y. Kim, S. Cheon, G.R. Yi, J.H. Cho, Halide welding for silver nanowire network electrode. *ACS Appl. Mater. Interfaces* **9**, 30779–30785 (2017)
43. T. Tokuno, M. Nogi, M. Karakawa, J. Jiu, T.T. Nge, Y. Aso, K. Suganuma, Fabrication of silver nanowire transparent electrodes at room temperature. *Nano Res.* **4**, 1215–1222 (2011)

Publisher's Note Springer Nature remains neutral with regard to jurisdictional claims in published maps and institutional affiliations.

Springer Nature or its licensor (e.g. a society or other partner) holds exclusive rights to this article under a publishing agreement with the author(s) or other rightsholder(s); author self-archiving of the accepted manuscript version of this article is solely governed by the terms of such publishing agreement and applicable law.